JGR Earth Surface

RESEARCH ARTICLE
10.1029/2024JF007761

Seismic Modeling of Bedload Transport in a Gravel-Bed Alluvial Channel

Loc Luong[1], Daniel Cadol[1], Susan Bilek[1], J. Mitchell McLaughlin[1], Jonathan B. Laronne[2,3], and Jens M. Turowski[4]

[1]Earth and Environmental Science, New Mexico Tech, Socorro, NM, USA, [2]Earth and Environmental Sciences, Ben Gurion University of the Negev, Beer Sheva, Israel, [3]Dead Sea Arava Science Center, Masada National Park, Dead Sea, Israel, [4]GFZ German Research Center for Geoscience, Telegrafenberg, Potsdam, Germany

Key Points:

- The Tsai et al. (2012, https://doi.org/10.1029/2011gl050255) model underestimates bedload flux at low water depth by 1–2 orders of magnitude in an alluvial channel
- We modified the original model to incorporate rolling and sliding by adjusting bedload impact frequency, velocity, and angle
- The modified model decreases flux error relative to observations to less than one order of magnitude across all measured water depths

Correspondence to:
L. Luong,
loc.luong@student.nmt.edu

Citation:
Luong, L., Cadol, D., Bilek, S., McLaughlin, J. M., Laronne, J. B., & Turowski, J. M. (2024). Seismic modeling of bedload transport in a gravel-bed alluvial channel. *Journal of Geophysical Research: Earth Surface*, *129*, e2024JF007761. https://doi.org/10.1029/2024JF007761

Received 29 MAR 2024
Accepted 12 SEP 2024

Author Contributions:
Conceptualization: Loc Luong, Daniel Cadol, Jonathan B. Laronne, Jens M. Turowski
Formal analysis: Loc Luong, Susan Bilek, J. Mitchell McLaughlin
Funding acquisition: Daniel Cadol, Susan Bilek, Jonathan B. Laronne
Investigation: Loc Luong, Daniel Cadol
Methodology: Loc Luong, Daniel Cadol, Susan Bilek
Resources: Jens M. Turowski
Supervision: Daniel Cadol, Jonathan B. Laronne
Visualization: Loc Luong
Writing – original draft: Loc Luong
Writing – review & editing: Daniel Cadol, Susan Bilek, J. Mitchell McLaughlin, Jonathan B. Laronne, Jens M. Turowski

Abstract Recent theoretical models and field observations suggest that fluvial bedload flux can be estimated from seismic energy measured within appropriate frequency bands. We present an application of the Tsai et al. (2012, https://doi.org/10.1029/2011gl050255) bedload seismic model to an ephemeral channel located in the semi-arid southwestern US and incorporate modifications to better estimate bedload flux in this environment. To test the model, we collected streambank seismic signals and directly measured bedload flux during four flash-floods. Bedload predictions calculated by inversion from the Tsai model underestimated bedload flux observations by one-to-two orders of magnitude at low stages. However, model predictions were better for moderate flow depths (>50 cm), where saltation is expected to dominate bedload transport. We explored three differences between the model assumptions and our field conditions: (a) rolling and sliding particles have different impact frequencies than saltating particles; (b) the velocity and angle of impact of rolling particles onto the riverbed differ; and (c) the fine-grained alluvial character of this and similar riverbeds leads to inelastic impacts, as opposed to the originally conceptualized elastic impacts onto rigid bedrock. We modified the original model to assume inelastic bed impacts and to incorporate rolling and sliding by adjusting the statistical distributions of bedload impact frequency, velocity, and angle. Our modified "multiple-transport-mode bedload seismic model" decreased error relative to observations to less than one order of magnitude across all measured flow conditions. Further investigations in other environmental settings are required to demonstrate the robustness and general applicability of the model.

Plain Language Summary The conveyance of sediments in rivers, especially of coarse-grained sediment on the riverbed, is a basic geomorphic mechanism influencing short-term river ecology, management, and engineering as well as long-term landscape evolution. To better predict bedload transport rates, researchers have used seismic sensors to record ground vibration due to the impacts of bedload particles on the riverbed. We revised a physics-based model developed by Tsai et al. (2012, https://doi.org/10.1029/2011gl050255) to estimate bedload sediment transport in an ephemeral channel in the semi-arid southwestern US. To test the model, we collected nearby seismic signals during flash floods and simultaneously monitored water depth and bedload transport at one-minute intervals. We modified the original model to better represent alluvial rivers by adding a representation of rolling and sliding particles to the hopping particles already considered in the physics of seismic waves generated by bedload transport. Our modified "multi-mode bedload seismic model" yields a better result compared to the original Tsai et al. (2012, https://doi.org/10.1029/2011gl050255) model in our test river. The modified model is not only applicable for the ephemeral channels on which this study is focused but also is potentially applicable to a wide range of river conditions in different environmental settings.

1. Introduction

Bedload transport is a fundamental geomorphic process that plays a crucial role in shaping landscapes, with far-reaching implications for other inter-disciplinary fields such as geomorphology, ecology, hydrology, river engineering, and water resources management. Sediment budgets are necessary in both perennial and ephemeral channels for a variety of applications, such as irrigation and floodplain engineering, reservoir sedimentation management, habitat restoration, and flood risk mitigation (Badoux et al., 2014; Garcia, 2008; Schleiss et al., 2016; Totschnig et al., 2011; Wilcock, 2004). Given this practical demand, many bedload transport models have been proposed (Ancey, 2020a). However, we are far from having a fully effective and predictive model of the underlying physics of fluvial bedload transport (Ancey, 2020b), in part due to its stochastic behavior

(Einstein, 1936; Furbish et al., 2012; Yager et al., 2018). For a long time, hydraulics-based modeling has been the primary tool for estimating bedload flux, with various studies presenting empirically derived estimates of average bedload transport rates under different geomorphic conditions (e.g., Meyer-Peter & Müller, 1948; Parker, 1990; Wilcock & Crowe, 2003; Yager et al., 2012). Most of these studies have failed to provide general applicability to a wide range of river conditions (e.g., roughness, armoring, grain size distribution (GSD)) or their predictive capability is not better than one order of magnitude (Ancey, 2020b; Schneider et al., 2015). One example of a complication besetting these efforts is the variable presence of winnowed "bed armor" layers, which may delay bed mobilization and which are prevalent in perennial rivers but rare in ephemeral channels (Laronne & Reid, 1993; Venditti et al., 2017).

A potential path around the challenges of hydraulics-based modeling is the widespread monitoring of bedload flux. Indirect methods for monitoring bedload transport—for example, hydrophones, pipe and plate microphones, geophones (e.g., Burtin et al., 2016; Geay et al., 2017; Gray et al., 2010; Rickenmann et al., 2014)—can serve as an alternative approach to dangerous and temporally limited manual direct sampling (e.g., Bunte & Abt, 2005; Bunte et al., 2008; Emmet, 1979) and costly continuously sampling installations (e.g., Reid et al., 1995). Moreover, several pioneering studies have demonstrated the potential of using seismic monitoring methods to quantify fluvial processes (e.g., Burtin et al., 2008; Farin et al., 2019; Gimbert et al., 2014; Govi et al., 1993; Hsu et al., 2011; Larose et al., 2015; Schmandt et al., 2013; Tsai et al., 2012) with respect to both theoretical and experimental aspects. In a benchmark study on fluvial seismology, Tsai et al. (2012) developed a framework to relate seismic data to bedload transport by modeling seismic energy produced by the impact of individual particles onto the riverbed and integrating across all grain size classes within the channel. Based upon this framework, others began relating event-induced seismic power to a variety of environmental processes based on the physics of impulsive events. For example, Gimbert et al. (2014) proposed a physical model for seismic noise generated by turbulence. Others (Farin et al., 2019; Kean et al., 2015; Lai et al., 2018; Yan et al., 2023) developed and improved models for debris flows, while Gimbert et al. (2019) further advanced the bedload seismic model. Seismic approaches have recently been used to record the seismic energy generated by bedload transport and turbulent flow in several regions worldwide (e.g., Bakker et al., 2020; Burtin et al., 2016; Chao et al., 2015; Lagarde et al., 2021; Polvi et al., 2020), demonstrating that not only acoustic (Antoniazza et al., 2023; Nasr et al., 2022) but also seismic approaches for monitoring fluvial processes may be deployed in diverse regions to study bedload transport, river morphology, and landscape evolution.

Seismic noise induced by bedload transport, turbulent flow, and other ambient processes such as wind and rain generate signals in distinctive frequency bands (e.g., Burtin et al., 2008; Gimbert et al., 2014; Tsai et al., 2012). As such, a physics-based model aimed at relating seismic signals to bedload flux may be an effective means to distinguish and isolate bedload transport from other fluvial processes. The original model for bedload (Tsai et al., 2012) assumes that the vertical component of the impact of particles on the riverbed dominates energy transfer. This model was constructed for rivers where the saltating mechanism of transport is assumed to be dominant under intense flows. Evaluation of this model in an ephemeral gravel-bed river has resulted in substantial overestimation of bedload flux (Lagarde et al., 2021). By comparing inverted bedload flux using the Tsai et al. (2012) model and field observations, Lagarde et al. (2021) explored the role of grain size both in seismic energy delivery and transport mode and found that large particles dominate energy transfer. Therefore, it is crucial to have appropriate constraints on the motion of the largest grains when inverting river seismic signals for bedload flux. To better model seismic noise generated by bedload transport, several subsequent studies assumed oblique impacts between mobile particles and stationary bed particles (Farin et al., 2019; Gimbert et al., 2019) with statistical distributions of the deviated plane of the impacts, calculated based on grain size distributions and assumed rounding. Gimbert et al. (2019) introduced a method to stochastically incorporate a hop time distribution (inverse of temporal impact frequency) that conceptually encompasses all three transport regimes (rolling, sliding, and saltating). Based on flume experiment data at the grain scale, the authors presented a wide distribution of hop times with a higher average impact frequency than predicted by previously existing saltation models (Sklar & Dietrich, 2004). Farin et al. (2019) developed a theoretical model for seismic signals generated by debris flows, in which they used the average downstream bedload velocity to characterize the impacts of debris onto a channel bed comprised of other rounded grains. Their approach of incorporating an irregular bed is also applicable to alluvial environments.

The Tsai et al. (2012) model was developed assuming a bedrock river environment, which we hereafter refer to as the "saltation-mode bedload seismic model." This model has opened a path for quantitative analysis of bedload

seismic signals and has been applied in a number of sites since its publication (e.g., Chao et al., 2015; Dietze et al., 2019; Roth et al., 2016; Schmandt et al., 2013). Yet, recent studies with high-quality benchmark data have demonstrated that the model does not fully capture all of the physical processes relevant in alluvial rivers (e.g., Bakker et al., 2020; Lagarde et al., 2021; Schmandt et al., 2017). We aim to generalize the model for alluvial conditions. First, we evaluate the Tsai et al. (2012) model in a sandy gravel-bed alluvial channel with extensive field observations. We then developed a modified model, termed "multi-mode bedload seismic model," with the goal of improving the quantification of bedload flux in this ephemeral environment. By combining recent theoretical advances (Farin et al., 2019; Gimbert et al., 2019; Tsai et al., 2012) and our field observations, we also aim to provide a sufficiently general model to extend to other environmental settings, such as gravel or boulder bed rivers.

2. Theoretical Background

The movement of bedload generates seismic noise on the riverbed. This propagates as seismic waves, where the resulting vibration or displacement can be picked up by a receiver. Bedload transport initiates ground motion that can be described by a source function (F), typically quantified by a force history. Green's function (G) quantifies the alterations of seismic waves as they travel along the path from the source to the receiver. A mathematical expression (Aki & Richards, 2002) describes ground displacement $s(t, \boldsymbol{x})$ at location $\boldsymbol{x} = \langle x, y, z \rangle$ by the convolution of a source $F(t, \boldsymbol{x}_0)$ at location $\boldsymbol{x}_0 = \langle x_0, y_0, z_0 \rangle$ with the Green's function $G(t, \boldsymbol{x}, \boldsymbol{x}_0)$:

$$s(t, \boldsymbol{x}) = F(t, \boldsymbol{x_0}) * G(t, \boldsymbol{x}, \boldsymbol{x_0}). \tag{1}$$

Using a Fourier transform, the ground velocity $\dot{u}(f, \boldsymbol{x})$ at location $\boldsymbol{x}$ is expressed in the frequency domain as:

$$\dot{u}(f, \boldsymbol{x}) = 2\pi i f \boldsymbol{F}(f, \boldsymbol{x_0})\, \boldsymbol{G}(f, \boldsymbol{x}, \boldsymbol{x_0}), \tag{2}$$

where $\boldsymbol{F}(f, \boldsymbol{x}_0)$ is Fourier's transform of $F(t, \boldsymbol{x}_0)$ and $\boldsymbol{G}(f, \boldsymbol{x}, \boldsymbol{x}_0)$ is Fourier's transform of $G(t, \boldsymbol{x}, \boldsymbol{x}_0)$, t denotes the time domain, f denotes the frequency domain, and i is an imaginary unit. One can arrive at an equation expressing the power spectral density (PSD) of the ground velocity $\dot{u}(f, \boldsymbol{x})$ in the frequency domain by employing the force history $\boldsymbol{F}(f, \boldsymbol{x}_0)$ to characterize the bedload impact onto riverbed, and the Green's function $\boldsymbol{G}(f, \boldsymbol{x}, \boldsymbol{x}_0)$ to describe seismic waves traveling through the ground.

Based on the physics of bedload transport, contact mechanics, and the theory of seismic waves traveling through the subsurface, Tsai et al. (2012) developed a mathematical relationship between the seismic signals generated by bedload transport and its flux. This allows for the estimation of bedload flux based on the seismic energy recorded by a seismometer located outside of a river. They assumed (a) Hertzian impacts (Hertz, 1882) for contacts between particles and the riverbed, (b) that particles that impact vertically and elastically on the riverbed mainly generate Rayleigh waves, (c) negligible rolling and sliding particles, (d) an infinitely long straight source of impacts, (e) impacts occur randomly in time, and (f) the impact rate is directly related to bedload flux (Lamb et al., 2008; Sklar & Dietrich, 2004). Hertzian impacts are characterized by contact times that are much shorter than the recording frequency. They are typically represented by a Dirac delta function, the Fourier transform of which is equal to one. This implies that the power spectra of Hertzian impacts encompass all frequencies. Rayleigh waves, one of the commonly observed seismic surface waves, exhibit an elliptical trajectory similar to ocean waves, thereby inducing both vertical and horizontal ground motion in the travel direction. This is in contrast to Love waves, which exhibit only horizontal motion transverse to the travel direction. Rayleigh waves are widely regarded as the predominant surface waves produced by bedload transport (Dammeier et al., 2011; Sánchez-Sesma et al., 2011). The seismic energy (P_v) generated per unit grain size class (D) based on Tsai et al. (2012) is expressed as

$$P_v(f, D) = \underbrace{\frac{C_1 W q_{bD} \overline{w}_s}{V_p U_b H_b}}_{\text{(I)}} \cdot \underbrace{\frac{\pi^2 f^3 m^2 {w_i}^2}{{\rho_s}^2 v_c^3 v_u^2}}_{\text{(II)}} \cdot \underbrace{\chi(\beta)}_{\text{(III)}}. \tag{3}$$

The parameters in Equation 3 have been named as in the original development of the Tsai et al. (2012) model and are listed in Table 1. Here, the Tsai et al. (2012) model can be interpreted as a product of three components labeled

Table 1
Parameters Used by Tsai et al. (2012) for Calculating Power Spectral Density From Bedload Flux

Model component	Parameters	Unit	Description of parameters	Source
Bedload impact frequency model	q_{bD}	m^2/s	Volumetric bedload flux	Dependent variable
	C_1	–	Constant, account for rise and fall time	Theory
	W	m	Average channel-bed width	Field data
	$\hat{w}_s$	m/s	Depth-average particle settling velocity	Empirical
	V_p	m^3	Particle volume	Field data
	U_b	m/s	Vertically averaged streamwise bedload velocity	Empirical
	H_b	m	Bedload layer height	Empirical
Seismic model	f	Hz	Frequency	Seismic data
	m	kg	Particle mass	Field data
	w_i	m/s	Particle speed	Empirical
	ρ_s	kg/m^3	Particle density	Field data
	v_c	m/s	Rayleigh-wave phase velocity	Field data
	v_u	m/s	Rayleigh-wave group velocity	Field data
Attenuation model	$\chi(\beta)$	–	Attenuation of seismic waves	Seismic data

in Equation 3: (I) a bedload impact frequency model that represents how bedload is transported by fluid flow and impacts the riverbed, (II) a seismic model that represents how seismic waves uniformly generated by bedload along the channel travel through the ground layers and are integrated at the receiver (seismometers), and (III) an attenuation model that represents how seismic wave amplitudes decay temporally and spatially.

3. Methods

3.1. Study Site Overview

The Arroyo de Los Pinos (ADLP), a direct tributary of the middle Rio Grande in New Mexico, USA, hosts a variety of instruments to monitor sediment and water flow during the summer monsoon season. Three Reid-type slot samplers (Reid et al., 1980) were placed in the arroyo bed for direct bedload monitoring in 2018, in conjunction with pressure transducers that record water depth and pipe microphones embedded in the channel upstream of the samplers that record bedload impacts (Halfi et al., 2020; Mizuyama et al., 2010; Stark et al., 2021). A broadband seismic station was installed in 2017 on the channel bank, and additional seismic nodes were installed during 2019–2022 (Bilek, McLaughlin, Cadol, Laronne, Stark, et al., 2023). The channel has an anastomosing morphology as it crosses the Pliocene and Pleistocene ancestral Rio Grande floodplain and alluvial fan deposits in the lower watershed (Stark et al., 2021). Near the confluence with the Rio Grande, where the morphology is constrained to a single channel by levees, the channel consists of a sand-and-gravel thalweg and somewhat coarser bars. The spatially averaged bed material consists of approximately 30% sand ($D < 2$ mm), 55% granules ($2 < D < 8$ mm), 10% medium-to-coarse gravel ($8 < D < 64$ mm), and 5% cobbles ($D > 64$ mm). For details of the sediment flux monitoring methods and grain size analysis, refer to Stark et al. (2021).

3.2. Seismic Data: PSD Calculation and Relevant Frequency Ranges

We used seismic data collected from a long-term broadband seismometer located ~20 m from the sediment samplers to compute the PSD during flood periods for comparison with the theoretical model PSD calculations. As an example, seismic data and a hydrograph from a flood (2021-07-05; year-month-day) demonstrate the increase in seismic power associated with the arrival of the flood over a range of frequencies (Figure 1). We computed the PSD of the vertical component of the seismic signals collected during floods by first removing the instrument response and then using Welch's method (Welch, 1967) with a window length of 2^{14} and a 50% window overlap. Median PSD was computed over 1-min windows; this is the PSD used for model comparison.

Seismic noise can arise from numerous sources besides bedload movement, including water flow, wind, or interactions between floodwater and vegetation (e.g., Gimbert et al., 2014; Schmandt et al., 2017). At the ADLP, we have previously studied and characterized various noise sources, from anthropogenic noise to concurrent fluvial

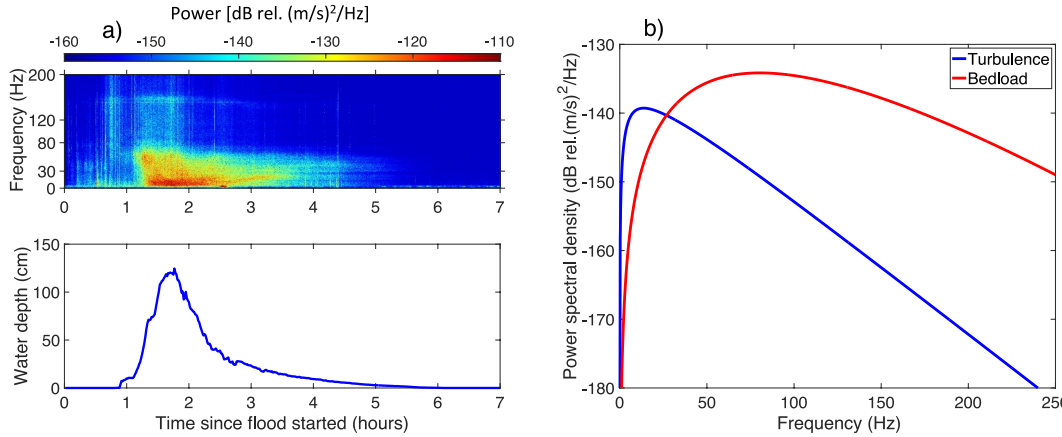

Figure 1. (a) Hydrograph (bottom) and spectrogram (top) for flood on the Arroyo de los Pinos starting at 22:00 on 2021-07-05, local time (4:00 on 2022-07-06, UTC time). (b) Power spectral density (PSD) based on the theoretical models of Tsai et al. (2012) for bedload transport and Gimbert et al. (2014) for turbulence. We used a 20 m source-receiver distance, hydrologic parameters measured at the monitoring station, and the grain size distribution of bedload trapped during this flood to produce the PSD curves.

and meteorological processes, such as turbulence, hydraulic jumps, rainfall, and thunder (McLaughlin et al., 2023). Frequency response is fundamentally dependent on attenuation, which is based on the distance between the river and seismic station, and which affects higher frequencies more than lower frequencies. At our field site, we comprehensively analyzed the frequency response to determine the optimum frequency bands generated by bedload transport (McLaughlin et al., 2023). Based on that site-specific analysis and previous studies that suggest that bedload transport-related seismic signals are typically observed at frequencies >15 Hz, particularly when the river-station distance is small (Roth et al., 2016; Schmandt et al., 2013, 2017), we focused on a 30–80 Hz frequency range for our tests of seismic-bedload models. This range of frequencies incorporates most of the range expected for bedload transport and excludes most frequencies that may be significantly influenced by confounding sources of seismic noise, such as seismic noise in the 1–10 Hz range that are from the interstate highway or railroad across the valley from the monitoring station or noise below 30 Hz that is from a nearby hydraulic jump (McLaughlin, 2022). This interpretation is consistent with theoretical predictions of seismic frequencies generated by bedload (Tsai et al., 2012) and turbulence (Gimbert et al., 2014) for our field site (Figure 1b). For a GSD and flow depth typical of the site, predicted bedload PSD begins to exceed turbulence PSD at ∼30 Hz.

We also observed that rainfall noise occurs in a broad window of frequency (e.g., 1–400 Hz) at 6 out of the 21 flow events from 2018 to 2023. At our field site, we have installed a rain gauge near the seismic sensor and have analyzed rainfall radar data for each event. McLaughlin (2022) compared the rainfall intensity with seismic PSD in different frequency bands and concluded that rainfall noise affects all recorded frequencies and thus needs to be carefully considered when analyzing seismic data for the purpose of bedload monitoring. However, the 30–80 Hz frequency band is not excessively influenced by rainfall and is therefore reasonable for this study.

3.3. Modification of the Physics-Based Model

To adapt the saltation-mode bedload seismic model (Tsai et al., 2012) to an alluvial setting, modifications can be applied to several of its components: impact frequency, impact angles on bed particles, and impact elasticity. Force due to particle impacts is assumed to be proportional to the particle terminal fall speed in the Tsai et al. (2012) model, whereas in the multi-mode bedload seismic model, we assume that force is proportional to downstream bedload speed. We assume inelastic impacts and account for oblique impact angles on the bed particles by integrating various angles, as described by Farin et al. (2019). We first begin by reviewing a key assumption in Tsai et al. (2012) model.

If impacts are assumed to be random in time, the PSD $P_v(D, f)$ for a unit grain size D of the ground velocity time series $\dot{u}(t,x)$ measured at a seismic station has the same spectral shape as the square of an individual impact transformed to the frequency domain, $\dot{u}(f, x)$, and an amplitude proportional to the number of impacts (Tsai

et al., 2012). Therefore, we can relate the PSD per unit grain size in the frequency domain to bedload flux and impact characteristics:

$$P_v(f,D) = \int_R R^D_{\text{impact}} |\dot{u}(f,x)|^2 dx, \tag{4}$$

where R is the length of the river, and R^D_{impact} is the total rate of impacts for grain size class D in a unit length of river, with $R^D_{\text{impact}} = n_D / t_D$, where n_D is the number of impacting particles of grain size D per unit length of river, and t_D is the characteristic timescale between impacts for grain size D (Tsai et al., 2012). We keep this fundamental assumption.

Lamb et al. (2008) previously noted that

$$R^D_{\text{impact}} = \frac{n_D}{t_D} = \frac{q_{bD} W}{V_p s}, \tag{5}$$

where q_{bD} is the volumetric sediment flux per unit width per unit grain size D, W is river width, V_p is particle volume, and s is the characteristic length scale between impacts.

A particle transported as bedload can experience three modes of transport: rolling, hopping, and sliding depending on hydraulic and river conditions (Gilbert, 1914). Tsai et al. (2012) focused on saltating particles. Instead, we use a probability distribution that represents the likelihood that a particle undergoes different transport modes. This could be conveniently done by relating the distribution of particle hop times to their transport mode. A shorter hop time indicates that particles are likely in a rolling or possibly sliding mode, with the time representing a period of time between impacts with bed protrusions rather than a true hop time, whereas a longer hop time indicates that particles are likely in a saltating mode. Small hop times can also occur due to multiple saltation impacts and ricochets, such as additional rebounds off nearby surfaces that occur after the initial bounce of a grain on the riverbed (Gimbert et al., 2019). Gimbert et al. (2019) included the probability density function of hop times between impacts in the Tsai et al. (2012) model. Their approach is described by

$$P_T(f,x) = \int_D \int_R \int_t p_t(t_D) \frac{n_D}{t_D} |\dot{u}(f,x)|^2 dt_D dx dD. \tag{6}$$

We can identify s with the hop length of saltating particles. Similarly, for a rolling particle, we can define s as the distance of rolling or sliding between distinct impacts onto bed elements such as grains or pockets. Rewriting Equation 5, we can solve for n_D as

$$n_D = \frac{q_{bD} W}{V_p \frac{s}{t_D}} = \frac{q_{bD} W}{V_p U_b} = \frac{p(D)\, q_b W}{V_p U_b}, \tag{7}$$

where U_b is the average stream-wise speed of bedload in all transport modes, and $p(D)$ is the GSD function. To quantify the characteristic length between impacts, we used the product of bedload velocity and hop time ($s = U_b t_D$). The characteristic length scale (s) varies based on the hop times and bedload velocity to represent different transport mechanisms (e.g., high values of s can be interpreted as saltation, low values of s can be interpreted as rolling or sliding). The uncertainty in this equation is amplified bidirectionally by both bedload velocity and hop time distribution. We estimated bedload velocity using empirical equations to be introduced later, while the hop time distribution is based on flume data from Gimbert et al. (2019).

Tsai et al. (2012) assumed impacts on a plane bed, but the average impact of particles onto a riverbed consisting of rounded grains can be estimated by using a coefficient f_j and averaged downstream bedload velocity U_b (Farin et al., 2019). This is given by

$$\boldsymbol{F_j}(f) = (1+\gamma) m U_b f_j, \tag{8}$$

where γ is a restitution coefficient equal to 0 for fully inelastic impacts and 1 for fully elastic impacts and m is the particle mass. f_j is a dimensionless speed ratio that accounts for the impulse directed in the normal direction relative to the impact plane between the mobile particle and the stationary riverbed particles.

Following previous authors (Aki & Richards, 2002; Farin et al., 2019; Gimbert et al., 2014; Tsai et al., 2012), we assume a horizontally homogenous medium and Rayleigh waves that decay with depth, enabling approximation of the displacement Green's function as a one-dimensional surface-wave propagation:

$$\boldsymbol{G}_{jz}(f,x;x_0) \approx N_{jz}\frac{k}{8\rho_s v_c v_u}\sqrt{\frac{2}{\pi kr}}e^{-\frac{\pi f r}{(v_u Q)}}, \tag{9}$$

where v_c is the Rayleigh-wave phase velocity, v_u is group velocity, k is angular wave number, r is source-to-receiver distance, Q is seismic quality factor (inverse of attenuation), and N_{jz} are dimensionless numbers describing the relative amplitude of the x-, y-, and z-dimensional components of ground motion (Tsai & Atiganyanun, 2014). Because we both model and analyze only vertical ground motion, we neglect the influence of Love waves.

The ground velocity in the frequency domain can then be expressed by substituting Equations 8 and 9 into Equation 2 as follows:

$$\dot{u}(f,x) = 2\pi i f\sum_j (1+\gamma)\, m U_b f_i N_{jz}\frac{k}{8\rho_s v_c v_u}\sqrt{\frac{2}{\pi kr}}e^{-\pi f r/(v_u Q)}, \tag{10}$$

where j stands for the force components in the x, y, and z directions.

Finally, substituting Equations 5 and 10 into Equation 4, we obtain a full parametric expression of the total PSD generated by particles impacting the riverbed:

$$P_T(f,x) = \int_D\int_R\int_t p_t(t_D)\,\frac{p(D)\,q_b W}{V_p U_b t_D}\left|2\pi i f\sum_j (1+\gamma) m U_b f_j N_{jz}\frac{k}{8\rho_s v_c v_u}\sqrt{\frac{2}{\pi kr}}e^{-\frac{\pi f r}{(v_u Q)}}\right|^2 dt_D x dD. \tag{11}$$

Equation 11 can be simplified using the following three assumptions: (a) the river is infinitely long and straight, (b) the approximated attenuation model $\chi(\beta)$ of Tsai et al. (2012) can be used, and (c) we focus on the vertical component of seismic energy generated by bedload (the N_{11} term). Note that in Equation 12, we used f_z to reduce the seismic power into a single average value according to oblique impact geometry and directions of impact (Farin et al., 2019). This yields:

$$P_T(f,x) = \int_D\int_t p_t(t_D)\cdot\frac{p(D)\,q_b W}{V_p U_b t_D}\cdot\left|N_{11}(1+\gamma)U_b f_z\right|^2\cdot\frac{\pi^2 f^3 m^2}{4\rho_s{}^2 v_c^3 v_u^2}\cdot\chi(\beta)\,dt_D dD. \tag{12}$$

These modifications are relevant to both the originally conceptualized bedrock setting, as well as our application to an alluvial setting. Because the new model (Equation 12) conceptually incorporates impacts from rolling, sliding, as well as saltating particles, we call it the "multiple-transport-mode bedload seismic model" to indicate that it may encompass all three modes of transport, and we use the term "multi-mode model" for short. Similarly, we refer to the original Tsai model as the "saltation-mode bedload seismic model" or simply "saltation-mode model." Although identifying the Tsai et al. (2012) model as the saltation-mode model might be construed to mean that it is most appropriate for saltation-only situations, this is not necessarily the case. The Gimbert et al. (2019) observations of complex and ricocheting hop impacts suggest that hop-time-based models, such as our multi-mode model, offer advantages even in cases where saltation is the only transport mode. But we selected the names based on the processes that are being conceptually incorporated into each model. To explore the relative performance of each approach, we tested the sensitivity of both models to variation in depth, grain size, hop time, and bedload velocity while keeping other model parameters constant.

3.4. Estimation of Average Bedload Velocity

The most uncertain parameters in the multi-mode model are (a) the characteristic time distribution (hop time or rolling time between impacts) and (b) stream-wise bedload velocity. To estimate the total PSD from Equation 12, one needs explicit distributions for the hop time and grain size. To allow general hop time and grain size distributions, we developed a script to compute total PSD numerically rather than analytically. We used a truncated lognormal distribution fitted to flume data from Gimbert et al. (2019) to obtain a hop time distribution and applied it to all grain sizes. We truncated the curve fit because of the limited range of results reported by Gimbert et al. (2019). In the final form, $P_T(f,x)$ scales linearly with stream-wise bedload velocity U_b. Thus, a valid constraint of this velocity is essential. Chatanantavet et al. (2013) presented a linear scaling relation of average stream-wise bedload velocity to average downstream water velocity, while others expressed the depth average stream-wise bedload velocity in terms of hydraulic variables (Gimbert et al., 2019; Julien & Bounvilay, 2013; Sklar & Dietrich, 2004). Yet another approach to constrain the average stream-wise bedload velocity is to estimate the average downstream velocity at certain depths using a logarithmic velocity profile (Bathurst, 1978; Keulegan, 1938; Von Kármán, 1931) and surface velocity observations. For comparison, we present several equations to estimate average bedload velocity. First, we use the relationship fitted by Sklar and Dietrich (2004) to a data compilation:

$$U_b = 1.56\sqrt{RgD}\left(\frac{\tau_*}{\tau_{c*}} - 1\right)^{0.56}. \tag{13}$$

Next, an empirical equation from Julien and Bounvilay (2013) estimates the stream-wise rolling bedload velocity using flume experiments for $1 < D < 30$ mm bedload:

$$U_b = 30.5\sqrt{RgD}\tau_*\left(\frac{D}{k_s}\right)^{0.583}. \tag{14}$$

Additionally, according to Gimbert et al. (2019), the relationship for average downstream cobble velocity is expressed by

$$U_b = 1.19\sqrt{RgD}\left(\frac{\tau_*}{\tau_{c*}} - 1\right)^{0.3}. \tag{15}$$

In the three equations, R, the submerged specific gravity, is equal to $\rho_s/\rho_f - 1$, where ρ_s ($\approx$2,700 kg/m^3) and ρ_f ($\approx$1,000 kg/m^3) are solid and fluid densities, respectively; g ($\approx$9.81 m/s^2) is gravitational acceleration; τ^* is the Shield parameter and is calculated as $\tau_* = u_*^2/RgD$; u^* is near-bed shear velocity calculated as $u_* = \sqrt{gH\sin\theta}$; θ is the channel slope angle; τ_c^* is the critical Shields parameter and is a function of water depth, grain size and channel slope (Lamb et al., 2008; Parker, 1990); and k_s is bed roughness, which we estimated to be three times the median grain size (Kamphuis, 1974). We did not directly monitor bedload velocity in the field. However, we deployed an electromagnetic current velocity meter 15 cm above the bed during one flow event. This instrument can provide an upper limit on bedload velocity. Based on this limit, we used Sklar and Dietrich (2004) and Julien and Bounvilay (2013) for estimating bedload velocity.

3.5. Inversion Scheme

We followed the inversion scheme of Lagarde et al. (2021) to invert bedload flux from seismic data. Assuming that the model adequately describes the physics of seismic signals generated by bedload transport, Lagarde et al. (2021) calculated PSD* using the Tsai model with the bedload flux term (q_b) factored out. In our application, the following equations were used to obtain the inverted bedload fluxes:

$$\mathrm{PSD}^* = \int_D \int_t p_t(t_D) \cdot \frac{p(D)\,W}{V_p U_b t_D} \cdot \left| N_{11}(1+\gamma) U_b f_j \right|^2 \cdot \frac{\pi^2 f^3 m^2}{4\rho_s{}^2 v_c^3 v_u^2} \cdot \chi(\beta)\, dt_D dD. \tag{16}$$

If the model accurately quantifies the physics of sediment transport, the PSD observed by the seismometer ($PSD_{observed}$) should equal the computed seismic PSD, P_T, equivalent to $q_b(PSD^*)$. Therefore, bedload flux can be calculated as the ratio between the observed seismic PSD and PSD*:

$$q_b = \frac{PSD_{observed}}{PSD^*}. \quad (17)$$

4. Results

4.1. The Saltation-Mode Model Results

In applying the saltation-mode model (Tsai et al., 2012), the predicted PSD is highly sensitive to elastic parameters, including rock density and the phase and group velocities of Rayleigh waves. For our gravel-bed alluvial channel, we conducted active source surveys at the site to determine a group velocity of ∼250 m/s and a phase velocity of ∼200 m/s at a reference frequency of 1 Hz (Bilek, McLaughlin, Cadol, Laronne, & Luong, 2023), following the calculation procedures of Lagarde et al. (2021). These are much slower than group and phase velocities reported for bedrock settings (Tsai et al., 2012), and are similar to the Bakker et al. (2020) results. Thus, the unconsolidated alluvium within and around the channel considerably reduces the observed seismic energy when compared to that for bedrock. We also used these surveys to estimate the seismic quality factor. The quality factor Q does vary slightly between 16 and 26 in the frequency range of 30–80 Hz, but for simplicity, we use Q ∼ 20 for our model as that is a reasonable estimate based on our site data and consistent with many other similar studies (Bakker et al., 2020; Bilek, McLaughlin, Cadol, Laronne, & Luong, 2023; Tsai et al., 2012).

The PSD predicted by the saltation-mode model strongly depends on the grain size diameter D; PSD is approximately proportional to D^3 (Farin et al., 2019; Tsai et al., 2012). Therefore, constraining the GSD is also essential to obtain an accurate inversion of bedload flux (Lagarde et al., 2021). To determine the GSD of our data set derived from a flow event on 05 July 2021, we visually fitted a log-transformed raised-cosine distribution (Tsai et al., 2012) to the active bedload grain size data of more than 10 sieved bedload samples collected in the Reid-type slot samplers during this event. The samples that were trapped during the event gave the most accurate representation of bedload in motion. The cumulative distribution function (cdf) was manually matched to the field GSD data, and the probability density function (pdf) was derived from the cdf (Figure 2a). Given the disproportionate influence of large grains (Lagarde et al., 2021; Turowski et al., 2015), we prioritized matching the cdf with the largest grain sizes in the manual selection of log-raised-cosine parameters. The median grain size of the bed material (not necessarily bedload in transport) at the station is approximately 5 mm. In the 05 July 2021 flow event, the median transported bedload grain size was ∼10 mm, approximately 10% of the sediment was sand (<2 mm), 80% was gravel (2–64 mm), and 10% was cobbles (64–256 mm). Using the log-raised-cosine GSD fit (Figure 2a), we inverted the bedload fluxes for the event using Equation 17 (Figure 2b). The inverted bedload fluxes are approximately one to two orders of magnitude smaller than our field measurements at low flow stages, but they begin to converge at the highest measured fluxes just before the sampling boxes fill (Figure 2b). The comparisons are only possible through the first ∼20 min of the flood because of the limited sampler capacity. The model yields bedload fluxes of about 20 kg m^{-1} s^{-1} at peak discharge, which is only slightly higher than any width-averaged flux rates measured hitherto at the station (Stark et al., 2021).

4.2. Sensitivity of the Saltation-Mode and Multi-Mode Models

We estimated N_{11} to be ∼0.352 and quality factor Q ∼20 (Bilek, McLaughlin, Cadol, Laronne, & Luong, 2023) based on active source studies at the site, following the procedure from Lagarde et al. (2021), and used $f_z = 0.539$ according to Farin et al. (2019) for estimating the average amount of seismic energy transferred to vertical ground motion from the oblique impacts. We calculated the PSD for both the multi-mode and saltation-mode models, in each case independently varying the values of D, H, t_D and U_b, and leaving all other parameters constant (Figure 3). In each PSD calculation, we used the same parameter values as Tsai et al. (2012), where sediment flux $q_b = 10^{-3}\, m^2/s$, river slope $\theta = 1.4°$, $W = 50$ m, source-receiver distance $r_0 = 600$ m, phase velocity $v_c = 1{,}295$ m/s, and group velocity $v_u = 945$ m/s. As expected, the total PSD varied considerably depending on the choice of grain size diameters. Our sensitivity analysis shows that modeled PSD varies from a few factors by water depth or to ∼1 to 2 orders of

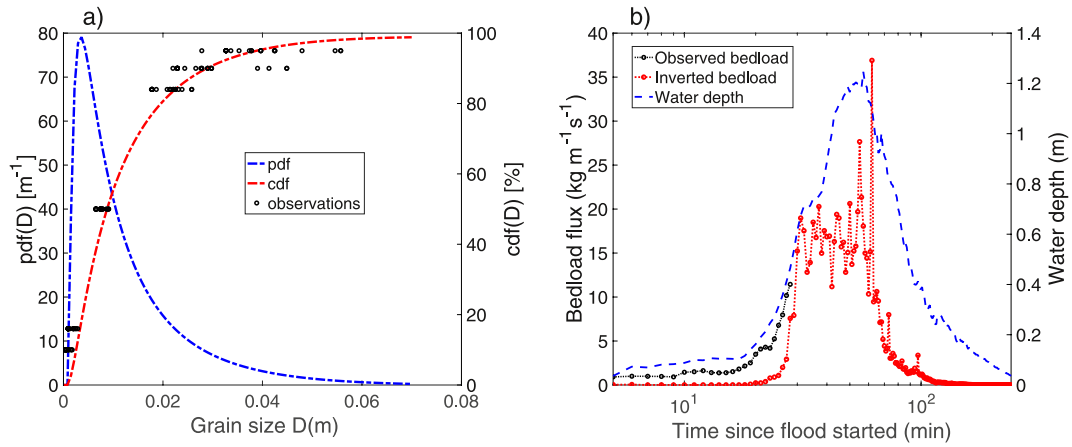

Figure 2. Results from applying the saltation-mode model (Tsai et al., 2012) to the 2021-07-05 flood. (a) Grain size distribution of bedload. (b) Time series of inverted and observed bedload flux. Note that observations ceased when the samplers filled.

magnitude by hydraulic and sediment parameters (e.g., grain size, hop time, bedload velocity) as well as by seismic parameters, such as group velocity, and phase velocity.

We also compared the PSD from the multi-mode model with the saltation-mode model (Tsai et al., 2012) at conditions closer to those found at our field station. We used a phase velocity $v_c \sim 250$ m/s, and group velocity $v_u \sim 200$ m/s at 1 Hz (Bilek, McLaughlin, Cadol, Laronne, & Luong, 2023). We calculated the PSD for four different stages of flow depth (0.3, 0.7, 1.2, and 2.0 m) in combination with four grain sizes (Figure 4). At low stages (<0.3 m) and for the same combination of parameters, the PSD generated by the multi-mode model is slightly larger than that generated by the saltation-mode model for $D = 3$ mm and is slightly smaller for $D \geq 5$ mm. From

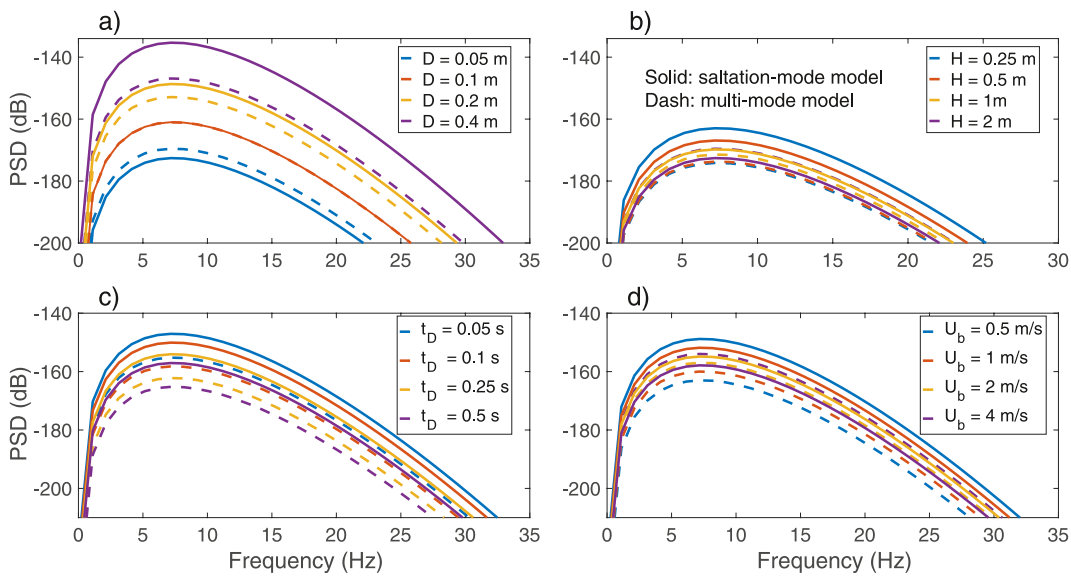

Figure 3. Sensitivity of the saltation-mode model (solid lines, Tsai et al., 2012) and multi-mode model (dashed lines) to variation in grain size D, flow depth H, hop time t_D, and average stream-wise bedload velocity U_b. We used a 600 m source-receiver distance for more direct comparison with the test case in Tsai et al. (2012). (a) Modeled power spectral density (PSD) according to varied grain size at a flow depth of 2 m. The saltation-mode model is shown with solid lines and the multi-mode model with dashed lines in all four plots. (b) Modeled PSD according to varied flow depth at grain size of 0.05 m. (c) Modeled PSD according to varied hop time with grain size of 0.1 m (same velocity for both models). (d) Modeled PSD according to varied bedload velocity with grain size of 0.1 m (same hop time for both models). Note that we used decibel units (dB), effectively creating a base 10 logarithmic scale. Solid lines are from the Tsai el al. (2012) model, and dashed lines are from this study.

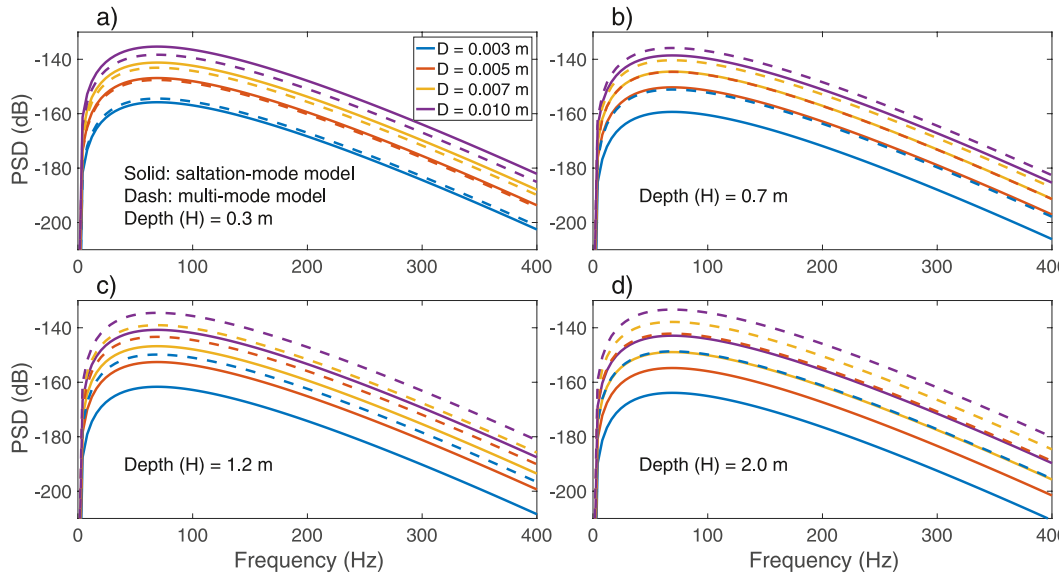

Figure 4. Comparison of power spectral density between the saltation-mode model (Tsai et al., 2012) and multi-mode model. For this comparison, we used a 20 m source-receiver distance, which is less than the value used in Figure 3 and is representative of our field station. For all plots, we considered grain sizes in the range 3–10 mm, the dominant grain sizes at our field station. (a) Flow depth of 0.3 m; (b) flow depth of 0.7 m; (c) flow depth of 1.2 m; (d) flow depth of 2.0 m. In all comparisons we used a fixed 0.15 s hop time. The saltation-mode model is shown with solid lines and the multi-mode model with dashed lines in all four plots.

medium to high flow depths ($H \geq 0.7$ m), the PSD generated by the multi-mode model is considerably larger than that generated by the saltation-mode model, especially for larger grains ($D = 10$ mm).

The discrepancy between the two models (Figures 3a and 4a) is mainly due to the different empirical equations used to estimate the rate and force of impacts. In the multi-mode model, the impact rate is determined by the bedload velocity and hop time, whereas in the saltation-mode model, it is determined by the terminal settling velocity and the bedload layer thickness. The impact force is determined by downstream bedload velocity in the multi-mode model, but terminal settling velocity in the saltation-mode model. In this comparison, we employed identical parameters (e.g., a flow depth of 2 m in Figure 3a or 0.3 m in Figure 4a) and chose a fixed hop time of 0.15 s in the multi-mode model. Depending on the hop time value, the multi-mode model can yield higher or smaller PSD compared to the saltation-mode model at certain grain size classes. For example, with a grain size of 0.05 m at a water depth of 2 m, PSD generated by the multi-mode model is higher than that generated by the saltation-mode model. However, as grain sizes increase, the saltation-mode model yields higher PSD than the multi-mode model; particularly, at D ∼0.1 m (Figure 3a) or D ∼0.005 m (Figure 4a) the trend switches from higher PSD for the multi-mode model to the saltation-mode model.

Based on the comparison of both models at our field site (Figure 4), we calculated the ratio of PSD between the multi-mode and saltation-mode models for different grain sizes (Figure 5). At high water depths (e.g., >0.7 m), the multi-mode model produces greater seismic power than the saltation-mode model for small grain sizes because the hop time is fixed at 0.15 s for all conditions in the multi-mode model, and greater depths produce higher bedload velocity leading to higher impact frequency and force. However, for the saltation-mode model, impact frequency and force are controlled by fall velocity, which is small for small grains. For sizes approaching 200 mm, the saltation-mode model produces greater PSD than that of the multi-mode model, as a result of higher impacting forces per impact. The tradeoff between more impacts in the multi-mode model versus greater energy per impact in the saltation-mode model begins to favor the saltation-mode model for larger grain sizes. At low water depth (e.g., <0.3 m), the multi-mode model produces less seismic power than the saltation-mode model even for small grains because the shear stress and bedload velocity decrease, resulting in lower calculated bedload impact velocity while fall velocity remains relatively constant as depth decreases. Thus, there is a transition or a crossover in Figure 5 from the multi-mode PSD being greater to the saltation-mode PSD being greater. As water depths decrease, the ratio $PSD_{\text{multi-mode model}}/PSD_{\text{saltation-mode model}}$ also decreases. For small grains (<4 mm), the

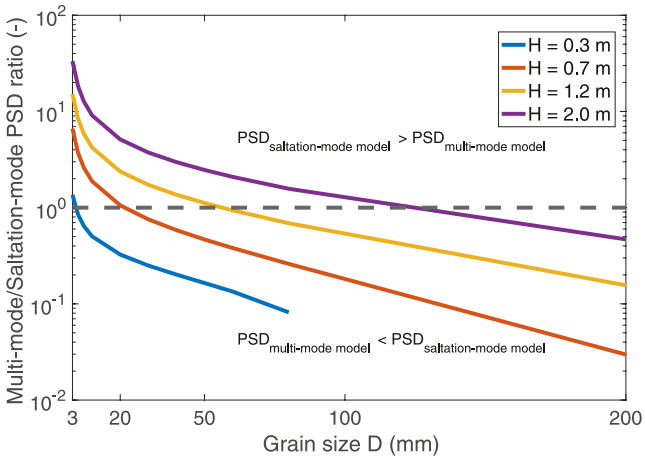

Figure 5. Ratio of power spectral density (PSD) between the multi-mode and saltation-mode models for different water depths. Model parameters are constrained using data from our field station. The seismic PSD of the multi-mode model is equal to the saltation-mode model at the dashed line.

multi-mode model produced more seismic power at all tested depths down to 0.3 m. Both models have the same peak frequencies (Figures 3 and 4) for the same seismic parameters (e.g., group and phase velocities, quality factor).

At our field site, we also monitored flow velocity using an electromagnetic current meter (ECM) and obtained a velocity of ∼2.5 m/s at 15 cm above the bed during a 40-cm-deep flow event. Our estimation of $U_b \sim 2$ m/s at 40 cm flow depth from the empirical equations is consistent with the upper constraint provided by the ECM data (Figure 6). For sand and small-gravel grain sizes, and from low stage up to a depth of 40 cm, the Julien and Bounvilay (2013) equation yields similar results to that of Sklar and Dietrich (2004). From medium to high water depths, the results of the Julien and Bounvilay equation substantially exceed those of the Gimbert et al. (2019) and the Sklar and Dietrich equations due to the unbounded limit of the expression (Figure 6). Hence, we used the Julien and Bounvilay (2013) equation for small flow depths (<0.4 m), where it was trained, and the Sklar and Dietrich (2004) equation for higher flow depths (>0.4 m).

4.3. Results From the Multi-Mode Model

We used a truncated lognormal distribution to represent the distribution of bedload hop times because it had a better visual fit to the hop-time curve derived from the data of Gimbert et al. (2019) than uniform, normal, truncated normal, or untruncated lognormal distributions. The long tail toward the right can capture the observed distribution that includes some long hops, but with a majority being relatively short (Figure 7). In the flume data from Gimbert et al. (2019), the hop times fall in the range of 0.03–0.50 s for pebbles and cobbles; these are an order of magnitude shorter than the empirical saltation equations used in Tsai et al. (2012). To estimate average stream-wise bedload velocity, we employed the equation proposed by Julien and Bounvilay (2013) for low and medium stages ($H < 40$ cm) when our bedload size was consistent with their training data, and for higher stages (40 cm < H), we used the Sklar and Dietrich (2004) equation. Inverted bedload fluxes from the multi-mode model were consistently smaller than the observations for the entire flood, but within a factor of two (Figure 7b).

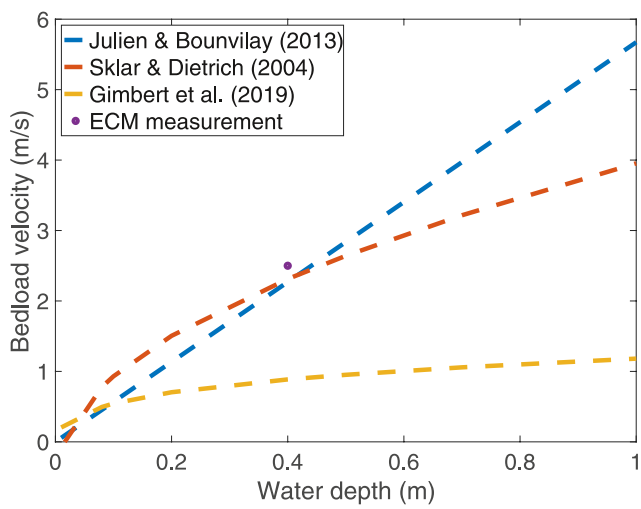

Figure 6. Empirical estimations of averaged streamwise bedload velocity (U_b). Field measurement of flow velocity was obtained with an electromagnetic current meter 15 cm above the bed at a water depth of 40 cm and represents an upper limit on bedload velocity. We used a grain size of 7 mm for this plot.

4.4. Comparison Between the Two Models With Additional Field Data

We also applied the inversion method (Equation 17) to seismic data from three additional flow events with strongly differing hydrographs to obtain bedload flux estimates (Figure 8). At low water depths (∼20–30 cm), the inverted bedload flux based on the saltation-mode model (blue points in Figure 8) overestimated the extent of seismic noise generated by bedload movement, hence underestimating the bedload flux compared with field observations (blue points in Figure 8). The multi-mode model also underestimated bedload flux relative to the observations for one flood (Figures 7b and 8b) but improved upon the Tsai et al. (2012) model, especially at low discharges when saltation is least likely (Figure 8). Mean relative error decreased from approximately 90%–74% using the multi-mode model. At high flows, for which we have no observational bedload flux data, the two models switched, and the saltation-mode model produced higher bedload estimates than the multi-mode model. Peak predictions of the saltation-mode model of up to 200 kg $s^{-1}m^{-1}$ were much higher than the maximum bedload transport rates of 12 kg $s^{-1}m^{-1}$ observed to this point (Stark et al., 2021), while peak predictions of the multi-mode model of up to 20 kg $s^{-1}m^{-1}$ were closer to observations (Figure 8). Predictions using the multi-mode model were within an order of magnitude of observations, except for some early periods in the 2021-07-05 and 2021-08-23 floods (shaded regions in Figure 8).

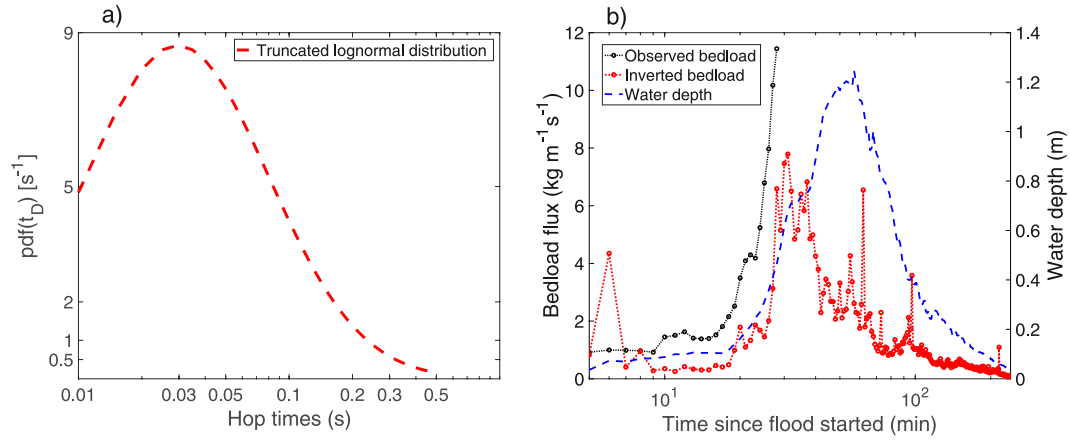

Figure 7. Results from the application of the multi-mode model to the 2021-07-05 flood. (a) Hop time distribution in log-log scale. (b) Time series of inverted and observed bedload flux.

5. Discussion

5.1. Assumptions and Uncertainty of the Multi-Mode Model

There are ∼22 independent parameters, only some of which are constrained by observations (Table 2) in the final expression of total PSD (P_T, Equation 12) as well as total PSD from the saltation-mode model (Tsai et al., 2012). Each of the parameters in the expression for P_T varies with respect to its physical range of constraints. Hence, constraining bedload flux from seismic noise is expected to have considerable uncertainty due to the high-dimensional parameter space. Moreover, the total PSD is subjected to large variation with respect to several model parameters. For example, PSD varies as v_c^5, causing model bias if v_c is not properly constrained.

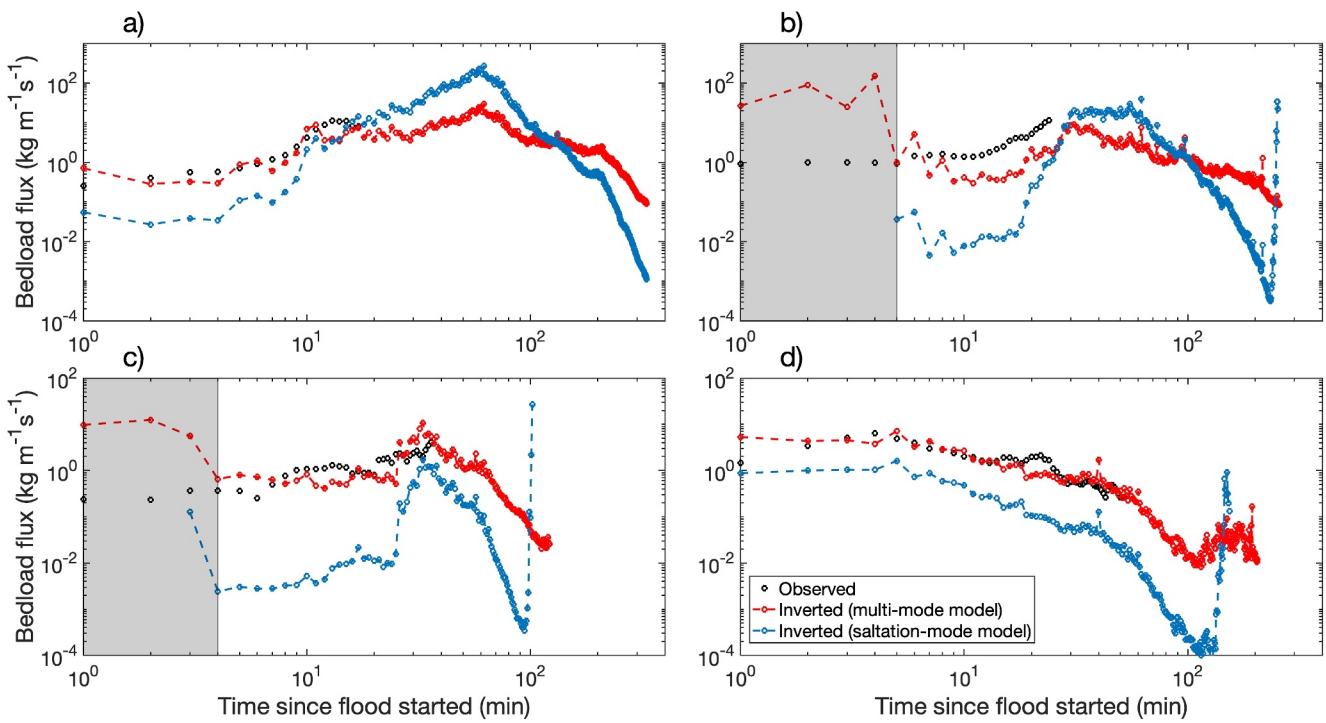

Figure 8. Inversion results and comparison with field observations for the saltation-mode model (Tsai et al., 2012) and multi-mode model (this study). (a) 2018-07-27 flood with peak water depth of ∼160 cm; (b) 2021-07-05 flood with peak water depth of ∼125 cm; (c) 2021-08-23 flood with peak water depth of ∼18 cm; (d) 2022-07-09 flood with peak water depth of ∼20 cm. Shaded areas in b and c are the beginning of the flood events where environmental and human signal contaminations are likely.

Table 2
Relative Constraints on Model Parameters

Model parameters	Description of parameters	Constraints	Influence on total PSD
$p_t(t_D)$	Hop time distribution	Poorly constrained	High influence
$p(D)$	Grain size distribution	Poorly constrained	High influence
s	Hop length	Poorly constrained	High influence
U_b	Averaged streamwise bedload velocity	Poorly constrained	High influence
$\chi(\beta)$	Attenuation of seismic waves	Modestly constrained	High influence
f	Frequency window	Modestly constrained	High influence
v_c	Rayleigh-wave group velocity	Modestly constrained	High influence
v_u	Rayleigh-wave phase velocity	Modestly constrained	High influence
N_{11}	Dimensionless number (Tsai & Atiganyanun, 2014)	Modestly constrained	Medium influence
ε	Variation coefficient for v_{c0}	Modestly constrained	Medium influence
γ	Restitution coefficient	Modestly constrained	Small influence
f_z	Fraction of vertical seismic energy	Modestly constrained	Small influence
Q	Quality factor	Well constrained	Medium influence
m	Particle mass	Well constrained	Small influence
r_0	Source-receiver distance	Well constrained	Small influence
ρ_s	Particle density	Well constrained	Small influence
W	River width	Well constrained	Small influence
V_p	Particle volume	Well constrained	Small influence

Additionally, the total PSD scales roughly with $D^{3.5}$ in the multi-mode model, and with D^3 in the saltation-mode model. To obtain a good prediction of bedload flux, one needs to have good constraints on these parameters. Here we qualitatively categorized model parameters based on our experience with the model and field data into three groups, thereby highlighting the uncertainty of each parameter: poorly constrained, modestly constrained, and well constrained (Table 2). The attenuation of seismic waves ($\chi(\beta)$) incorporates influence from several other parameters, including source-receiver distance, Rayleigh wave speed (v_{c0}) at reference frequency ($f_0 \sim 1$ Hz), quality factor Q_0 at reference frequency, and variation coefficient ε for v_{c0} (Tsai et al., 2012). Rayleigh-wave group and phase velocities vary with f, v_{c0}, and ε; and $\chi(\beta)$ scales roughly with f^5 (Tsai et al., 2012).

We implemented a key modification in the calculation of the frequency of bedload impact. In the saltation-mode model, Tsai et al. (2012) used the terminal settling velocity of bedload to estimate the force of impacts, and used it along with downstream bedload velocity to estimate impact frequency. We found that under low-stage flow conditions ($H < 20$ cm), when saltation is least likely, the saltation-based seismic model underestimated transport rates by $\sim$ 1–2 orders of magnitude (Figure 8). Presumably, the assumption of saltation was invalid (Table 2). At increasing flow depths, the shear threshold for gravel transport is exceeded, and even though gravel also rolls at this stage, the improving empirical estimation of bedload velocity or bedload layer height brings the bedload estimate from the saltation-mode model more in line with observations. The multi-mode model assumes empirical impact time spacing (Gimbert et al., 2019) at all stages; additionally, we use a more accurate estimate of bedload velocity for small particles based on Julien and Bounvilay's (2013) equation for low stages. In other words, in the multi-mode model, the impact rate decreases linearly with increasing bedload velocity for a constant flow depth, and the impact force increases to the second power of bedload velocity. In contrast, in the saltation-mode model (Tsai et al., 2012), impact velocity is the fall velocity slightly modulated by bedload layer height. As a result, an increase in flow depth increases bedload velocity and decreases impact frequency, while leaving the impact force relatively unchanged. This results in a decreased seismic energy with increasing stage for the saltation-mode model, as shown in Figure 3b, whereas in the multi-mode model, seismic energy increases with stage, consistent with field observations.

For a given characteristic impact length scale (s), the impact rate (n_D/t_D) is inversely proportional to the average stream-wise bedload velocity (U_b) in the multi-mode model. Nevertheless, the impact force is proportional to the

velocity squared. Hence, in Equation 12, PSD scales linearly with averaged stream-wise bedload velocity (Figure 3d). This can be interpreted as any bedload flux occurring over a unit area of a riverbed generating seismic signals, such that the power spectra follow a straight-line with respect to U_b. To obtain a good prediction of bedload flux from inversion, it is critical to constrain bedload velocity or, at the least, the average water velocity, which is higher than the upper limit of bedload velocity. Currently, field constraints of bedload velocity are rare. We have used several empirical equations (Equations 13–15) to estimate U_b (Figure 7). Future analyses could also consider additional similar equations (for example, Ashida & Michiue, 1972; Fernandez Luque & Van Beek, 1976; Niño et al., 1994). To obtain appropriate constraints of bedload velocity at other sites, one may need to select appropriate empirical equations suitable to the hydraulics or apply relevant data from flume experiments.

In Gimbert et al.'s (2019) flume experiments, the hop time distributions for gravel and cobble grain sizes were in the range 0.03–0.50 s. At a bedload velocity of 2 m/s, these hop times translate to 0.06–1 m between impacts. We expected bedload particles at our field site to travel within these hop lengths up to medium water depth (~50 cm), since the riverbed is mainly comprised of sand-and-gravel particles with a 5–6 mm median grain size, though abundant cobbles and some boulders were mobilized in the four studied flow events. We also extrapolated the hop time distribution down to 0.01 s at our field site to include larger grain sizes, as large particles would have smaller hop times.

In general, there are four difficult-to-constrain parameters to obtain an accurate estimate of bedload flux: average stream-wise bedload velocity (U_b), hop time distribution ($p_t(t_D)$), GSD ($p(D)$), and seismic phase velocity (v_c). We consider the hop time distribution and bedload velocity to be the most uncertain. Although we obtained good bedload predictions, further testing and investigations are required to validate these parameterizations and apply the multi-mode model to a wider range of fluvial settings.

5.2. Interpretation of Results From the Multi-Mode Model

The multi-mode model (this study) generally produced higher seismic power than the saltation-mode model (Tsai et al., 2012) for grain size classes at our site (Figure 5) for medium to high flow depth (Figures 8a and 8b), depths for which we do not have direct bedload flux measurements. In the scenario of bedload overestimation (e.g., Lagarde et al., 2021, and probably high flow depths at our field site), the multi-mode model would bring the inverted bedload closer to reality because at a given observed seismic PSD, the modeled PSD (Equation 16) is inversely proportional to bedload flux. At low flow depths at our site, the multi-mode model produced smaller seismic power than the saltation-mode model (Figure 5), resulting in a more accurate match between inverted bedload flux and observations than the saltation-mode model (Figures 8c and 8d). The results from the multi-mode model differ by a factor of ~2–3 from observations, whereas they deviate by 1–2 orders of magnitude from the saltation-mode model. We interpret this improvement to be due to the incorporation of rolling by using a hop time distribution that represents the likelihood of a particle engaging in different modes of transport. Further, the impacting forces of bedload on the riverbed may be more accurately represented by the average stream-wise bedload velocity U_b. Due to limited availability of hop time distribution data (Gimbert et al., 2019), in this study, we assumed that the hop time distribution is uniform across all particle sizes. If hop time distributions were available for several grain sizes, it would enable the incorporation of the distinct hop time distributions for each grain size in the model. Because larger grains dominate the generation of seismic signals, it is most important to accurately quantify them. The hop time distribution used here is derived from cobble-sized "smart rocks" (synthetic rocks with embedded accelerometers; e.g., Pretzlav et al., 2021), and thus would represent the largest particles in motion at most of our measured flows.

To invert bedload flux from seismic signals, we used a fixed GSD for both the saltation-model and multi-mode models. The GSD (Figure 2a) represents the bedload texture from the beginning of flood sediment sampling up to a water depth of ~40 cm. Bedload texture is unknown at higher water depths or during peak stages of medium to large flow events due to the limitations of the sampler capacity. We assumed that the GSD obtained from samplers during flood events represents the bedload particles in motion at our field location. The model can, in principle, deal with varying grain sizes over the course of a flood event. We expected that during high flows, coarser grains are mobilized than we assumed in our example calculations. This leads to higher seismic powers due to bedload in forward modeling, and, conversely, lower bedload fluxes when inverting a given signal.

At the beginning of flow events ($H < 10$ cm), there is considerable variation (Figure 8) in the seismic noise recorded near the river, likely due to near-river processes such as rain, thunder, or movements of the research

team. We often observed rainfall occurring before the flood bores arrived at the monitoring station; indeed, rainfall generates energy in a very wide 1 ∼ 400 Hz frequency band (McLaughlin et al., 2023; Roth et al., 2016). Hence, bedload inversions from both models might sometimes be too high because of non-bedload additions to seismic energy that contaminate the input signal. We also anticipate that the arrival of bore-fronts, as in the 2022-07-09 event, generates more seismic noise than subsequent portions of the flood because turbulence and shear stresses are higher (e.g., Chanson & Docherty, 2012; Thappeta et al., 2023). The bore-fronts often have higher velocities, and the initial interactions between fluid and solid phases with the riverbed create turbulence at the front of the flood, leading to additional seismic noise. Together, these factors suggest that the variability of the inverted bedload estimate at the beginning of floods (the gray areas of Figure 8) may result due to signals that are poorly correlated with bedload flux, and thus should be excluded.

5.3. Discussion of the Saltation-Mode Model and Implications for the Multi-Mode Model

The saltation-mode model (Tsai et al., 2012) underestimates bedload flux by ∼ 1–2 orders of magnitude at low flow depths at our site, yields results in good agreement with our field data at moderate flow depths, and yields high bedload fluxes at high stages for which we do not have field data (Figure 8). The saltation-mode model produced higher PSD than the multi-mode model for grain sizes greater than ∼50 mm (Figure 5). We expect a change in grain size to occur when the bars become mobilized or when shear stresses reach a sufficient magnitude to initiate motion of large particles (Wilcock et al., 1996), as saltation meanwhile becomes progressively more prevalent. This suggests that as water depth increases, the saltation-mode model becomes more suitable, but the GSD data becomes less reliable. As a result, we anticipate that the saltation-mode model is less applicable when the largest particles are rolling and more applicable when they saltate, that is, at very high-water stages. At the ADLP field site, this corresponds to stages of ∼1 m and above.

We expect that there are several potential reasons for the discrepancy between the prediction by the saltation-mode model (Tsai et al., 2012) and observed data (Figures 2 and 8). First, the riverbed is comprised of thick alluvial sediments, in contrast to the bedrock channel conceptualized in the original model development. Hence, seismic energy is lost due to the inelastic impact of sediment on the fine-grained substratum (Tullos & Reid, 1969). However, this is only expected to alter the modeled seismic energy by, at most, a factor of one-half, since elastic rebound doubles the calculated energy compared to a perfect inelastic collision. In the multi-mode model, the restitution term γ (e.g., Farin et al., 2019) is used to quantify the degree of inelastic impacts. Second, the saltation-mode model ignores rolling and sliding particles, which, based on observations by researchers standing in the channel during moderate flows, is likely to be a common type of bedload transport at our station. Moreover, the original bedload impact frequency model may not accurately represent the impact rate of particles on the riverbed. Under the same hydraulic conditions, rolling particles impact the bed more frequently than saltating particles, although each impact transfers less energy (Tsakiris et al., 2014). Previous analyses (Turowski et al., 2015; Turowski & Rickenmann, 2009) as well as the analysis presented here indicate that in the case of rolling gravel, the impact frequency is more important in this tradeoff and leads to higher seismic energy per unit distance traveled for rolling particles. Further, the impact of saltating particles onto the riverbed is hindered by the limitation of terminal fall velocity due to fluid drag, while rolling particles can accelerate with an increase in flow velocity. The comparison of seismic energy generated by rolling versus saltating particles is complicated because different grain sizes and shapes can experience different dominant transport mechanisms at a given flow condition (Tsakiris et al., 2014; Turowski & Rickenmann, 2009). For example, at water depths ∼40 cm, coarse gravels (>16 mm) are likely to roll, while sand and granules (2–8 mm) are likely to be in the saltation mode. An equation that depicts the relative fraction of rolling and saltating modes as a function of transport stage (e.g., Auel et al., 2017) could be used to differentiate seismic energy produced by rolling and saltating particles. Furthermore, a particle can also undergo different transport mechanisms depending on the hydraulics and riverbed characteristics. For example, a given gravel size class may saltate in a relatively deep flow but roll in shallower water, and rough riverbeds may increase turbulence and promote saltation when a particle is mobilized above the roughness elements. Finally, the focus on the vertical component of impacts onto the riverbed is reasonable as a starting point to derive the first-order relationship. But this assumes a planar bed, and in alluvial rivers the impacts of particles are more complicated as the bed is comprised of grains that receive impacts in a variety of generally oblique geometries (Farin et al., 2019; Lajeunesse et al., 2010). Hence, in the multi-mode model we use oblique impacts as suggested previously (Farin et al., 2019; Gimbert et al., 2019). In general, we suggest that the saltation-mode model may be applicable to rivers during floods where the predominance of saltation is a reliable

assumption. The multi-mode model is applicable to alluvial channels with active sand-gravel beds or perennial rivers where bedload particles are likely to roll, slide, and saltate. This also includes bedrock rivers at water discharges when turbulence and bedload fluxes are not very high.

6. Conclusions

The objective of this study was to evaluate the saltation-mode model (Tsai et al., 2012) in a different environment than the original high-energy setting. We aimed to examine model performance in estimating bedload flux from seismic data and to propose modifications to enhance the capacity of the model to match field data. These modifications involve altering assumptions about impact elasticity, impact angles, impact velocity, and impact frequency, leading to an adjusted derivation of the model. Based on our results (Figure 8), the focus on the vertical component of entrained grain motion to determine impact force by saltation may not be valid; instead, we assume oblique impact onto riverbeds consisting of other rounded grains, as implied by other studies that continued development of the Tsai et al. (2012) model (Farin et al., 2019; Gimbert et al., 2019). At our field site, the original model underestimated bedload at low to medium stages compared to field data, and potentially overestimated flux at peak stages. Overall performance of the multi-mode model (Figures 7 and 8) is in reasonable agreement with observations and improves over the predictions of the saltation-mode model.

The multi-mode model is not only applicable for the ephemeral channels on which this study is focused but also has the potential for application to a wide range of river conditions and different environmental settings. For example, to constrain bedload flux in bedrock rivers where the GSD mainly contains gravel and coarser particles, one can use an appropriate hop time distribution that represents the time interval at which these grains impact on the riverbed.

Data Availability Statement

Hydrologic data, including time-series stages, stream flow, bedload flux, and shear stress, are available at the Reclamation Information Sharing Environment (RISE). The data collected from the Arroyo de los Pinos can be accessed at the following URL: https://data.usbr.gov/catalog/4407. The four floods analyzed here are additionally archived in Luong, Stark, et al., 2024 (data set). Seismic data are from Bilek, 2024 (data set). All the codes for the saltation-mode model (Tsai et al., 2012) and the multi-mode model, as well as for reproducing results in this study, can be downloaded from Luong, Cadol, et al., 2024 (software). Seismic data were processed with the ObsPy library in Python; all figures were made in MATLAB R2022a.

Acknowledgments

Research support was provided by the US Bureau of Reclamation S&T program (project 9781, PI David Varyu) and sediment station construction was funded by the Albuquerque Area Office of Reclamation. Seismic monitoring and additional student support were funded by NSF grant EAR-1852794. Field data collection was assisted by (in chronological order) Kyle Stark, Madeline Richards, Zachary Chavez, Kelsey Romero, Sharllyn Pimentel, Sandra Glasgo, Rebecca Moskal, and Roheel Pashtoon. The authors thank Victor Tsai and two anonymous reviewers for their constructive comments and suggestions that improved the manuscript.

References

Aki, K., & Richards, P. G. (2002). *Quantitative seismology* (2nd ed., p. 700). University Science Books.

Ancey, C. (2020a). Bedload transport: A walk between randomness and determinism. Part 1. The state of the art. *Journal of Hydraulic Research*, *58*(1), 1–17. https://doi.org/10.1080/00221686.2019.1702594

Ancey, C. (2020b). Bedload transport: A walk between randomness and determinism. Part 2. Challenges and prospects. *Journal of Hydraulic Research*, *58*(1), 18–33. https://doi.org/10.1080/00221686.2019.1702595

Antoniazza, G., Dietze, M., Mancini, D., Turowski, J. M., Rickenmann, D., Nicollier, T., et al. (2023). Anatomy of an alpine bedload transport event: A watershed-scale seismic-network perspective. *Journal of Geophysical Research: Earth Surface*, *128*(8), e2022JF007000. https://doi.org/10.1029/2022JF007000

Ashida, K., & Michiue, M. (1972). Study on hydraulic resistance and bed-load transport rate in alluvial streams. In *Proceedings of the Japan Society of Civil Engineers*, (Vol. 206, pp. 59–69). Japan Society of Civil Engineers. https://doi.org/10.2208/jscej1969.1972.206_59

Auel, C., Albayrak, I., Sumi, T., & Boes, R. M. (2017). Sediment transport in high-speed flows over a fixed bed: 1. Particle dynamics. *Earth Surface Processes and Landforms*, *42*(9), 1365–1383. https://doi.org/10.1002/esp.4128

Badoux, A., Andres, N., & Turowski, J. M. (2014). Damage costs due to bedload transport processes in Switzerland. *Natural Hazards and Earth System Sciences*, *14*(2), 279–294. https://doi.org/10.5194/nhess-14-279-2014

Bakker, M., Gimbert, F., Geay, T., Misset, C., Zanker, S., & Recking, A. (2020). Field application and validation of a seismic bedload transport model. *Journal of Geophysical Research: Earth Surface*, *125*(5), e2019JF005416. https://doi.org/10.1029/2019JF005416

Bathurst, J. C. (1978). Flow resistance of large-scale roughness. *Journal of the Hydraulics Division*, *104*(12), 1587–1603. https://doi.org/10.1061/JYCEAJ.0005114

Bilek, S. (2024). Seismic Data From Arroyo de los Pinos experiment [Dataset]. *Zenodo*. https://doi.org/10.5281/zenodo.10818970

Bilek, S., McLaughlin, J. M., Cadol, D., Laronne, J. B., & Luong, L. (2023). Characterization of Green's Function Parameters for Seismic-based Bedload Predictions: Application to Arroyo de los Pinos, NM Bedload Observatory. In *AGU Fall Meeting Abstracts*. Abstract S41A-07, 2023 Fall Meeting, AGU, San Francisco. 11-15 Dec.

Bilek, S. L., McLaughlin, J. M., Cadol, D., Laronne, J. B., Stark, K., Luong, L., & Varyu, D. (2023). *Overview of bedload estimates based on seismic monitoring at the ephemeral Arroyo de los Pinos tributary of the Rio Grande, New Mexico*. SedHyd Conference, 2023. Retrieved from https://www.sedhyd.org/2023Program/s123.html

Bunte, K., & Abt, S. R. (2005). Effect of sampling time on measured gravel bed load transport rates in a coarse-bedded stream. *Water Resources Research*, *41*(11), W11405. https://doi.org/10.1029/2004WR003880

Bunte, K., Abt, S. R., Potyondy, J. P., & Swingle, K. W. (2008). A comparison of coarse bedload transport measured with bedload traps and Helley-Smith samplers. *Geodinamica Acta*, *21*(1), 53–66. https://doi.org/10.3166/ga.21.53-66

Burtin, A., Bollinger, L., Vergne, J., Cattin, R., & Nábělek, J. L. (2008). Spectral analysis of seismic noise induced by rivers: A new tool to monitor spatiotemporal changes in stream hydrodynamics. *Journal of Geophysical Research*, *113*(B5), B05301. https://doi.org/10.1029/2007JB005034

Burtin, A., Hovius, N., & Turowski, J. M. (2016). Seismic monitoring of torrential and fluvial processes. *Earth Surface Dynamics*, *4*(2), 285–307. https://doi.org/10.5194/esurf-4-285-2016

Chanson, H., & Docherty, N. J. (2012). Turbulent velocity measurements in open channel bores. *European Journal of Mechanics - B: Fluids*, *32*, 52–58. https://doi.org/10.1016/j.euromechflu.2011.10.001

Chao, W. A., Wu, Y. M., Zhao, L., Tsai, V. C., & Chen, C. H. (2015). Seismologically determined bedload flux during the typhoon season. *Scientific Reports*, *5*(1), 1–8. https://doi.org/10.1038/srep08261

Chatanantavet, P., Whipple, K. X., Adams, M. A., & Lamb, M. P. (2013). Experimental study on coarse grain saltation dynamics in bedrock channels. *Journal of Geophysical Research: Earth Surface*, *118*(2), 1161–1176. https://doi.org/10.1002/jgrf.20053

Dammeier, F., Moore, J. R., Haslinger, F., & Loew, S. (2011). Characterization of alpine rockslides using statistical analysis of seismic signals. *Journal of Geophysical Research*, *116*(F4), F04024. https://doi.org/10.1029/2011JF002037

Dietze, M., Lagarde, S., Halfi, E., Laronne, J. B., & Turowski, J. M. (2019). Joint sensing of bedload flux and water depth by seismic data inversion. *Water Resources Research*, *55*(11), 9892–9904. https://doi.org/10.1029/2019WR026072

Einstein, H. A. (1936). Der geschiebetrieb als wahrscheinlichkeitsproblem (Doctoral dissertation, ETH Zurich).

Emmet, W. (1979). A field calibration of the sediment trapping characteristics of the Helley-Smith bedload sampler. *U.S. Geological Survey, Open File Report 79-411*. https://doi.org/10.3133/pp1139

Farin, M., Tsai, V. C., Lamb, M. P., & Allstadt, K. E. (2019). A physical model of the high-frequency seismic signal generated by debris flows. *Earth Surface Processes and Landforms*, *44*(13), 2529–2543. https://doi.org/10.1002/esp.4677

Fernandez Luque, R., & Van Beek, R. (1976). Erosion and transport of bed-load sediment. *Journal of Hydraulic Research*, *14*(2), 127–144. https://doi.org/10.1080/00221687609499677

Furbish, D. J., Haff, P. K., Roseberry, J. C., & Schmeeckle, M. W. (2012). A probabilistic description of the bed load sediment flux: 1. Theory. *Journal of Geophysical Research*, *117*(F3), F03031. https://doi.org/10.1029/2012JF002352

Garcia, M. (2008). *Sedimentation engineering. Processes, measurements, modelling and practice*. American Society Civil Engineers. https://doi.org/10.1061/9780784408148

Geay, T., Belleudy, P., Gervaise, C. H., Habersack, J., Aigner, A., Kreisler, H., et al. (2017). Passive acoustic monitoring of bedload flux in a large gravel bed river. *Journal Geophysical Research - Earth Surface*, *122*(2), 528–545. https://doi.org/10.1002/2016JF004112

Gilbert, G. K. (1914). *The transportation of debris by running water (No. 86)*. US Government Printing Office. Retrieved from https://pubs.usgs.gov/publication/pp86

Gimbert, F., Fuller, B. M., Lamb, M. P., Tsai, V. C., & Johnson, J. P. (2019). Particle transport mechanics and induced seismic noise in steep flume experiments with accelerometer-embedded tracers. *Earth Surface Processes and Landforms*, *44*(1), 219–241. https://doi.org/10.1002/esp.4495

Gimbert, F., Tsai, V. C., & Lamb, M. P. (2014). A physical model for seismic noise generation by turbulent flow in rivers. *Journal of Geophysical Research: Earth Surface*, *119*(10), 2209–2238. https://doi.org/10.1002/2014JF003201

Govi, M., Maraga, F., & Moia, F. (1993). Seismic detectors for continuous bed load monitoring in a gravel stream. *Hydrological Sciences Journal*, *38*(2), 123–132. https://doi.org/10.1080/02626669309492650

Gray, J. R., Laronne, J. B., & Marr, J. D. (2010). *Bedload-surrogate monitoring technologies* (p. 37). US Department of the Interior, US Geological Survey.

Halfi, E., Paz, D., Stark, K., Reid, I., Dorman, M., & Laronne, J. B. (2020). Innovative mass-based calibration of bedload flux in rare flash flood events in semi-arid ephemerals. *Earth Surface Processes and Landforms*, *45*(14), 3510–3524. https://doi.org/10.1002/esp.4988

Hertz, H. (1882). Ueber die Berührung fester elastischer Körper. Retrieved from https://home.uni-leipzig.de/pwm/web/download/Hertz1881.pdf

Hsu, L., Finnegan, N. J., & Brodsky, E. E. (2011). A seismic signature of river bedload transport during storm events. *Geophysical Research Letters*, *38*(13), L13407. https://doi.org/10.1029/2011GL047759

Julien, P. Y., & Bounvilay, B. (2013). Velocity of rolling bed load particles. *Journal of Hydraulic Engineering*, *139*(2), 177–186. https://doi.org/10.1061/(ASCE)HY.1943-7900.0000657

Kamphuis, J. W. (1974). Determination of sand roughness for fixed beds. *Journal of Hydraulic Research*, *12*(2), 193–203. https://doi.org/10.1080/00221687409499737

Kean, J. W., Coe, J. A., Coviello, V., Smith, J. B., Mc- Coy, S. W., & Arattano, M. (2015). Estimating rates of debris flow entrainment from ground vibrations. *Geophysical Research Letters*, *42*(15), 6365–6372. https://doi.org/10.1002/2015GL064811

Keulegan, G. H. (1938). *Laws of turbulent flow in open channels*. U. S. Dept. of Commerce, National Bureau of Standards, Research Paper RP1151. Retrieved from https://nvlpubs.nist.gov/nistpubs/jres/21/jresv21n6p707_A1b.pdf

Lagarde, S., Dietze, M., Gimbert, F., Laronne, J. B., Turowski, J. M., & Halfi, E. (2021). Grain-size distribution and propagation effects on seismic signals generated by bedload transport. *Water Resources Research*, *57*(4), e2020WR028700. https://doi.org/10.1029/2020WR028700

Lai, V. H., Tsai, V. C., Lamb, M. P., Ulizio, T. P., & Beer, A. R. (2018). The seismic signature of debris flows: Flow mechanics and early warning at Montecito, California. *Geophysical Research Letters*, *45*(11), 5528–5535. https://doi.org/10.1029/2018GL077683

Lajeunesse, E., Malverti, L., & Charru, F. (2010). Bed load transport in turbulent flow at the grain scale: Experiments and modeling. *Journal of Geophysical Research*, *115*(F4), F04001. https://doi.org/10.1029/2009JF001628

Lamb, M. P., Dietrich, W. E., & Sklar, L. S. (2008). A model for fluvial bedrock incision by impacting suspended and bed load sediment. *Journal of Geophysical Research*, *113*(F3), F03025. https://doi.org/10.1029/2007JF000915

Laronne, J. B., & Reid, I. (1993). Very high rates of bedload sediment transport by ephemeral desert rivers. *Nature*, *366*(6451), 148–150. https://doi.org/10.1038/366148a0

Larose, E., Carrière, S., Voisin, C., Bottelin, P., Baillet, L., Guéguen, P., et al. (2015). Environmental seismology: What can we learn on earth surface processes with ambient noise? *Journal of Applied Geophysics*, *116*, 62–74. https://doi.org/10.1016/j.jappgeo.2015.02.001

Luong, L., Cadol, D., Bilek, S., McLaughlin, M., Laronne, J., & Turowski, J. (2024). Seismic modeling of bedload transport in a sandy gravel-bed alluvial channel [Software]. *Zenodo*. https://doi.org/10.5281/zenodo.13356758

Luong, L., Stark, K., Cadol, D., Laronne, J., & Varyu, D. (2024). Seismic modeling of bedload transport in a gravel-bed alluvial channel [Dataset]. *Zenodo*. https://doi.org/10.5281/zenodo.13357002

McLaughlin, J. M. (2022). Characterization and optimization of seismic methods for use in ephemeral river studies (Master's thesis).

McLaughlin, J. M., Bilek, S. L., Cadol, D., Laronne, J. B., Luong, L., & Varyu, D. (2023). *Field methods and instrument types: Considerations for using seismic methods to monitor bedload in sand-rich gravel bed ephemeral channels*. SedHyd Conference. Retrieved from https://www.sedhyd.org/2023Program/s148.html

Meyer-Peter, E., & Müller, R. (1948). Formulas for bed-load transport. In *IAHSR 2nd meeting, Stockholm, appendix 2*. IAHR. Retrieved from https://repository.tudelft.nl/record/uuid:4fda9b61-be28-4703-ab06-43cdc2a21bd7

Mizuyama, T., Laronne, J. B., Nonaka, M., Sawada, T., Satofuka, Y., Matsuoka, M., et al. (2010). *Calibration of a passive acoustic bedload monitoring system in Japanese mountain rivers* (Vol. 5091, pp. 296–318). US Geological Survey Scientific Investigations Report. Retrieved from https://pubs.usgs.gov/sir/2010/5091/papers/Mizuyama-passive.pdf

Nasr, M., Geay, T., Zanker, S., & Recking, A. (2022). A physical model for acoustic noise generated by bedload transport in rivers. *Journal of Geophysical Research: Earth Surface*, *127*(1), e2021JF006167. https://doi.org/10.1029/2021JF006167

Niño, Y., García, M., & Ayala, L. (1994). Gravel saltation: 1. experiments. *Water Resources Research*, *30*(6), 1907–1914. https://doi.org/10.1029/94WR00533

Parker, G. (1990). Surface-based bedload transport relation for gravel rivers. *Journal of Hydraulic Research*, *28*(4), 417–436. https://doi.org/10.1080/00221689009499058

Polvi, L. E., Dietze, M., Lotsari, E., Turowski, J. M., & Lind, L. (2020). Seismic monitoring of a subarctic river: Seasonal variations in hydraulics, sediment transport, and ice dynamics. *Journal of Geophysical Research: Earth Surface*, *125*(7), e2019JF005333. https://doi.org/10.1029/2019JF005333

Pretzlav, K. L., Johnson, J. P., & Bradley, D. N. (2021). Smartrock transport from seconds to seasons: Shear stress controls on gravel diffusion inferred from hop and rest scaling. *Geophysical Research Letters*, *48*(9), e2020GL091991. https://doi.org/10.1029/2020GL091991

Reid, I., Laronne, J. B., & Powell, D. M. (1995). The Nahal Yatir bedload database: Sediment dynamics in a gravel-bed ephemeral stream. *Earth Surface Process and Landforms*, *20*(9), 845–857. https://doi.org/10.1002/esp.3290200910

Reid, I., Layman, J. T., & Frostick, L. E. (1980). The continuous measurement of bedload discharge. *Journal of Hydraulic Research*, *18*(3), 243–249. https://doi.org/10.1080/00221688009499550

Rickenmann, D., Turowski, J. M., Fritschi, B., Wyss, C., Laronne, J., Barzilai, R., et al. (2014). Bedload transport measurements with impact plate geophones: Comparison of sensor calibration in different gravel-bed streams. *Earth Surface Processes and Landforms*, *39*(7), 928–942. https://doi.org/10.1002/esp.3499

Roth, D. L., Brodsky, E. E., Finnegan, N. J., Rickenmann, D., Turowski, J. M., & Badoux, A. (2016). Bed load sediment transport inferred from seismic signals near a river. *Journal of Geophysical Research: Earth Surface*, *121*(4), 725–747. https://doi.org/10.1002/2015JF003782

Sánchez-Sesma, F. J., Weaver, R. L., Kawase, H., Matsushima, S., Luzón, F., & Campillo, M. (2011). Energy partitions among elastic waves for dynamic surface loads in a semi-infinite solid. *Bulletin of the Seismological Society of America*, *101*(4), 1704–1709. https://doi.org/10.1785/0120100196

Schleiss, A. J., Franca, M. J., Juez, C., & De Cesare, G. (2016). Reservoir sedimentation. *Journal of Hydraulic Research*, *54*(6), 595–614. https://doi.org/10.1080/00221686.2016.1225320

Schmandt, B., Aster, R. C., Scherler, D., Tsai, V. C., & Karlstrom, K. (2013). Multiple fluvial processes detected by riverside seismic and infrasound monitoring of a controlled flood in the Grand Canyon. *Geophysical Research Letters*, *40*(18), 4858–4863. https://doi.org/10.1002/grl.50953

Schmandt, B., Gaeuman, D., Stewart, R., Hansen, S. M., Tsai, V. C., & Smith, J. (2017). Seismic array constraints on reach-scale bedload transport. *Geology*, *45*(4), 299–302. https://doi.org/10.1130/G38639.1

Schneider, J. M., Rickenmann, D., Turowski, J. M., Bunte, K., & Kirchner, J. W. (2015). Applicability of bed load transport models for mixed-size sediments in steep streams considering macro-roughness. *Water Resources Research*, *51*(7), 5260–5283. https://doi.org/10.1002/2014WR016417

Sklar, L. S., & Dietrich, W. E. (2004). A mechanistic model for river incision into bedrock by saltating bed load. *Water Resources Research*, *40*(6). https://doi.org/10.1029/2003WR002496

Stark, K., Cadol, D., Varyu, D., & Laronne, J. B. (2021). Direct, continuous measurements of ultra-high sediment fluxes in a sandy gravel-bed ephemeral river. *Geomorphology*, *382*, 107682. https://doi.org/10.1016/j.geomorph.2021.107682

Thappeta, S. K., Johnson, J. P., Halfi, E., Storz-Peretz, Y., & Laronne, J. B. (2023). Bed shear stress in experimental flash flood bores over dry beds and over flowing water: A comparison of methods. *Journal of Hydraulic Engineering*, *149*(4), 04023001. https://doi.org/10.1061/JHEND8.HYENG-13029

Totschnig, R., Sedlacek, W., & Fuchs, S. (2011). A quantitative vulnerability function for fluvial sediment transport. *Natural Hazards*, *58*(2), 681–703. https://doi.org/10.1007/s11069-010-9623-5

Tsai, V. C., & Atiganyanun, S. (2014). Green's functions for surface waves in a generic velocity structure. *Bulletin of the Seismological Society of America*, *104*(5), 2573–2578. https://doi.org/10.1785/0120140121

Tsai, V. C., Minchew, B., Lamb, M. P., & Ampuero, J. P. (2012). A physical model for seismic noise generation from sediment transport in rivers. *Geophysical Research Letters*, *39*(2), L02404. https://doi.org/10.1029/2011GL050255

Tsakiris, A. G., Papanicolaou, A. T. N., & Lauth, T. J. (2014). Signature of bedload particle transport mode in the acoustic signal of a geophone. *Journal of Hydraulic Research*, *52*(2), 185–204. https://doi.org/10.1080/00221686.2013.876454

Tullos, F. N., & Reid, A. C. (1969). Seismic attenuation of Gulf Coast sediments. *Geophysics*, *34*(4), 516–528. https://doi.org/10.1190/1.1440028

Turowski, J. M., & Rickenmann, D. (2009). Tools and cover effects in bedload transport observations in the Pitzbach, Austria. *Earth Surface Processes and Landforms*, *34*(1), 26–37. https://doi.org/10.1002/esp.1686

Turowski, J. M., Wyss, C. R., & Beer, A. R. (2015). Grain size effects on energy delivery to the streambed and links to bedrock erosion. *Geophysical Research Letters*, *42*(6), 1775–1780. https://doi.org/10.1002/2015GL063159

Venditti, J. G., Nelson, P. A., Bradley, R. W., Haught, D., & Gitto, A. B. (2017). Bedforms, structures, patches, and sediment supply in gravel-bed rivers. *Gravel-bed rivers: Processes and disasters*, 439–466. https://doi.org/10.1002/9781118971437.ch16

Von Kármán, T. (1931). *Mechanical similitude and turbulence (No. 611)*. National Advisory Committee for Aeronautics. Retrieved from https://ntrs.nasa.gov/citations/19930094805

Welch, P. (1967). The use of fast Fourier transform for the estimation of power spectra: A method based on time averaging over short, modified periodograms. *IEEE Transactions on Audio and Electroacoustics*, *15*(2), 70–73. https://doi.org/10.1109/TAU.1967.1161901

Wilcock, P. R. (2004). Sediment transport in the restoration of gravel-bed rivers. In *Critical transitions in water and environmental resources management* (pp. 1–11). https://doi.org/10.1061/40737(2004)433

Wilcock, P. R., Barta, A. F., Shea, C. C., Kondolf, G. M., Matthews, W. G., & Pitlick, J. (1996). Observations of flow and sediment entrainment on a large gravel-bed river. *Water Resources Research*, *32*(9), 2897–2909. https://doi.org/10.1029/96WR01628

Wilcock, P. R., & Crowe, J. C. (2003). Surface-based transport model for mixed-size sediment. *Journal of Hydraulic Engineering*, *129*(2), 120–128. https://doi.org/10.1061/(ASCE)0733-9429(2003)129:2(120)

Yager, E. M., Turowski, J. M., Rickenmann, D., & McArdell, B. W. (2012). Sediment supply, grain protrusion, and bedload transport in mountain streams. *Geophysical Research Letters*, *39*(10), L10402. https://doi.org/10.1029/2012GL051654

Yager, E. M., Venditti, J. G., Smith, H. J., & Schmeeckle, M. W. (2018). The trouble with shear stress. *Geomorphology*, *323*, 41–50. https://doi.org/10.1016/j.geomorph.2018.09.008

Yan, Y., Tang, H., Hu, K., Turowski, J. M., & Wei, F. (2023). Deriving Debris-Flow Dynamics From Real-Time Impact-Force Measurements. *Journal of Geophysical Research: Earth Surface*, *128*(3), e2022JF006715. https://doi.org/10.1029/2022JF006715